Welding in the World (2023) 67:2703–2714
https://doi.org/10.1007/s40194-023-01614-3

RESEARCH PAPER

Increase of electrode life in resistance spot welding of aluminum alloys by the combination of surface patterning and thin-film diffusion barriers

S. Brechelt[1] · H. Wiche[1] · J. Junge[1,2] · R. Gustus[1] · H. Schmidt[1,2] · V. Wesling[3]

Received: 31 August 2023 / Accepted: 17 October 2023 / Published online: 27 October 2023

Abstract
When resistance spot welding aluminum alloys, high electrode forces are required to reduce the electrical contact resistances between the electrodes and the sheet metals. The high contact resistances and the resulting thermal load cause extensive degradation of the electrode working faces. Weld spatter occurs after only a few weld cycles, significantly reducing the quality of the weld. Conventional resistance welding machines are limited in terms of maximum electrode force and weld current. As a result, weld quality and electrode life are inadequate. The aim is to increase the achievable electrode life by surface patterning the electrode working faces and creating thin-film diffusion barriers by physical vapor deposition (PVD). Patterning is intended to penetrate the oxide layers of the aluminum sheets and increase the proportion of electrically conductive contact areas. The different influences of patterning by particle blasting and contour turning will be investigated. As a further approach, thin-film diffusion barriers of up to 3 µm are deposited on the electrodes to prevent direct Al-Cu contact. Therefore, metallic coating materials (Ni and W) and an electrically highly conductive ceramic coating material (TiB2) are investigated. The combination of electrode patterning and thin-film diffusion barriers is tested in electrode life studies. It is shown that these modified electrode working faces can limit degradation effects and contribute to an increase in electrode life. In addition, the weld quality can be improved compared to the reference condition.

Keywords Resistance spot welding · Electrode life · Aluminum alloy · Surface patterning · Diffusion barrier

1 Introduction

Resistance spot welding (RSW) is primarily used in automotive body production due to its high efficiency, short cycle times, and good gap-bridging abilities. The cost-effectiveness of this joining process depends significantly on the achievable electrode life. Electrode life is defined as the

Recommended for publication by Commission III - Resistance Welding, Solid State Welding, and Allied Joining Process

✉ S. Brechelt
sascha.brechelt@tu-clausthal.de

H. Wiche
sekretariat@czm.tu-clausthal.de

J. Junge
sekretariat@czm.tu-clausthal.de

R. Gustus
sekretariat@czm.tu-clausthal.de

H. Schmidt
sekretariat@czm.tu-clausthal.de

V. Wesling
office@isaf.tu-clausthal.de

[1] Clausthal University of Technology, Centre of Material Technology, Leibnizstraße 9, 38678 Clausthal-Zellerfeld, Germany

[2] Clausthal University of Technology, Institute of Metallurgy, Robert-Koch-Straße 42, 38678 Clausthal-Zellerfeld, Germany

[3] Clausthal University of Technology, Institute of Welding and Machining, Agricolastraße 2, 38678 Clausthal-Zellerfeld, Germany

number of achievable weld cycles before the electrode caps need to be replaced or reworked. By RSW of uncoated steel materials, ~6000 weld cycles can be achieved. Zn-coated steel materials lower the achievable electrode life to ~3000 weld cycles [1]. The RSW of aluminum alloys leads to rapid damage of applied electrodes, which severely limits the electrode life depending on the abort criterion [2]. In the welding process, the natural oxide layer of aluminum leads to high temperatures in the electrode/sheet contact area and accelerates various damage mechanisms on the electrode working face. Therefore, the economic viability by RSW aluminum alloys is limited.

In this paper, modifications of electrode working faces are presented which address a reduction of the degradation rate and which consequently target an increase of the achievable electrode life. Mechanical patterning of the electrode working faces is expected to contribute to the destruction of the electrically insulating aluminum oxide layers and to reduce the resulting process temperatures in the electrode/sheet contact area. In addition, thin-film diffusion barriers are deposited on electrode working faces to prevent direct Al-Cu contact.

The aim is to demonstrate that the suggested modifications of electrode working faces can preserve the defined properties of the electrodes over an extended lifetime before the quality criteria of implemented joints are undercut. As a result, the suitability of conventional resistance welding machines with limited performance capability for the processing of aluminum alloys is intended to be achieved as well.

2 The methodology of resistance spot welding of aluminum alloys

Due to the high degradation rate in RSW of aluminum alloys, various technical approaches exist to increase the achievable electrode life. One of the common technical approaches targets the destruction of the aluminum oxide layer to improve the weldability. This can be achieved by mechanical removal of the oxidized sheet surface by grinding or by chemical etching with NaOH [3]. However, due to the increased surface roughness of the machined surfaces, local current density maxima can occur at the electrode/sheet contact. As a result, an increase in the degradation rate of the electrode working faces is possible. For this reason, chemical pretreatment of the sheets (e.g., etching) is preferable to mechanical methods (e.g., grinding) [4].

Patterning of electrode working faces also leads to an increase in the area of electrically conductive contacts to the sheet material. Due to the relative movements between the patterned electrode working faces and the sheet materials, a local destruction of the oxide layer can be achieved. Therefore, surface patterning promises a sustained reduction in electrical contact resistance [5]. The patterning can be realized by particle blasting or by contour turning [6]. In particular, multi-ring contours generated by contour turning promise to reduce the contact resistance and the amount of heat transferred in the electrode/sheet contact [7].

Diffusion barriers on electrode working faces have been investigated so far in different compositions and layer thicknesses. Thus, patents exist for diffusion-inhibiting geometric inserts [8] or claddings [9] in or on electrodes to avoid direct Al-Cu contact. However, an industrial use of diffusion-inhibiting inserts or claddings is not known. Furthermore, investigations exist to generate monolithic layers or composite layer systems by means of electro-spark deposition (ESD) in the layer thickness range of 50–100 µm [10]. However, it is noted in [11] that higher barrier layer thicknesses also lead to higher electrical resistances and lower heat conduction, which means that preferably, thin diffusion barrier layers should be aimed for.

The objective of this paper is, therefore, to investigate the influence of electrode patterning on the welding process (RSW) of aluminum alloys. In addition, physical vapor deposition (PVD) is used to generate thin-film diffusion barriers, which will contribute to slowing down the degradation effects.

3 Degradation mechanisms of electrode working faces

During the welding process, the electrode working faces are in direct contact with the sheet materials. High mechanical and thermal loads occur in the electrode/sheet contact, resulting in continuous degradation of the working faces. With an increasing number of weld cycles, reactive diffusion processes occur at the contact area. This results in a significant reduction in the electrical and thermal conductivity of the electrode working faces. This is due to the formation of alloys and intermetallic phases in the Al-Cu system with high electrical resistances. The continuous degradation of the electrode working faces is shown in Fig. 1.

Due to the Peltier effect, the weld nugget is shifted in the direction of the anode (Fig. 1a). As a result, the thermal load of the anode side is higher. A tactile measurement of the temperatures occurring in the electrode/sheet contact is not possible due to the high current densities. An optical measurement of the temperature is also not possible due to the welding position not being visible. However, the maximum temperatures occurring in the welding process can be estimated on the basis of the microstructure condition in the joint cross-section. A total of three temperature fields can be defined: the transition from the liquidus to the solidus area (I) exists at ~649 °C for the alloy AlMg3. Complete

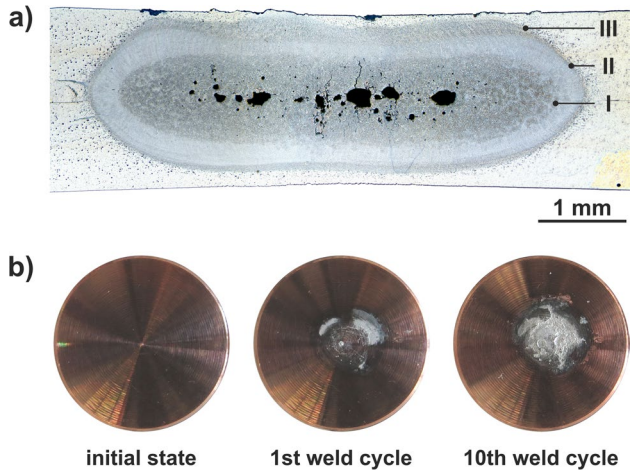

Fig. 1 Resistance spot welding: **a** etched cross-section (NaOH)—2 × 1 mm AlMg3 and **b** degradation of electrode working face (anode) after one and ten weld cycles

solidification (II) is reached at ~617 °C. In the outer area, the heat-affected zone (III) surrounds the weld nugget. The approximation of the temperatures from areas I and II is made from the binary phase diagram Al-Mg [12]. The weld nugget reaches the outer surface of the sheet material partially. As a result, local temperatures of > 617 °C can be expected at the outer sheet surface. Already after the first weld cycle, Al-Cu alloys and intermetallic phases are formed at the electrode working face (Fig. 1b). The propagation of these phases occurs continuously with each subsequent weld cycle. These degraded components of the electrode working face can be divided into different areas (Fig. 2).

In area I (Fig. 2a), local melting of the electrode working face occurs. At the expected local temperatures of > 617 °C in the electrode/sheet contact area, first phases of the alloy AlMg3 are in the molten state. Due to the direct contact with the electrode, local melting of the electrode material is initiated by lowering the liquidus area [13]. Below this temperature, solid-state diffusion occurs in area II. In the region of solid-state diffusion, two primary intermetallic phases are formed (Fig. 2b). The thickness of these layers varies significantly from 500 to 3500 nm. An analysis of these layers by energy-dispersive X-ray spectroscopy (EDX) line scans gives the relative concentration change of the elements Cu and Al across the layers. From the results, the formation of the Θ-phase (Al67Cu33 - ϑ_{melt} = 591 °C) and the δ-phase (Al40Cu60 - ϑ_{melt} = 958 °C) is suggested [13, 14]. Due to the high mechanical and thermal loads in the material region, partial cracking occurs between areas I and II. A breakout of these areas leads to pitting effects of the electrode working face (Fig. 2c).

4 Experimental procedure

4.1 Test facilities

The welding experiments are carried out on a conventional Nimak C-50 resistance spot welding machine with a medium-frequency inverter (111 kVA). The electrode caps of the material CuCr1Zr have the geometry according to ISO 5821 A0-16-20-100. The welding process is monitored by an online measuring system (HKS Weld Analyst). For each weld, the weld current, voltage, partial voltages between each boundary surface (electrode/sheet and sheet/sheet), and electrode force are recorded. The sampling rate is 58 kHz for each measurement channel.

The thin-film diffusion barrier layers are generated by physical vapor deposition (PVD). The Cemecon CC800-9 CUSTOM coating system allows the deposition of metallic and ceramic coatings. In addition to a classical DC sputter process, the layer density and the bonding to the substrate

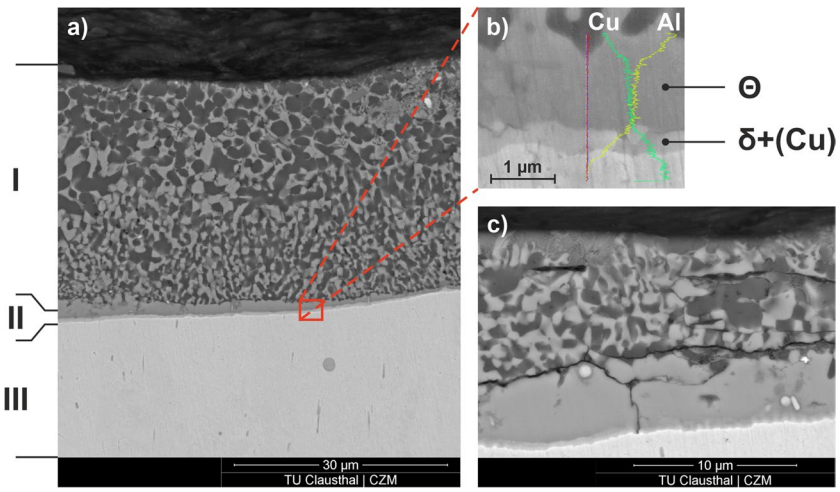

Fig. 2 Electrode degradation: **a** degraded electrode working face in cross-section, **b** EDX line scan of intermetallic phase region II, and **c** partial cracking between areas I and II

material can be further increased by high-power impulse magnetron sputtering (HIPIMS).

Investigations by grazing incidence X-ray diffractometry (GI-XRD) were done using a Bruker D8 DISCOVER diffractometer (Cu Kα, 40 keV, 40 mA) at an incidence angle of 3°.

4.2 Patterning of electrode working faces

The patterning of electrode working faces promises both to increase the electrode life and to improve the quality of the joints. By destroying the aluminum oxide layer, the contact resistance in the electrode/sheet contact is reduced, and local current density maxima are avoided. As a result, the thermal load of the electrode working face is reduced. In addition, the homogenization of the current density should help to reduce the formation of imperfections in the weld nugget. Patterning can be implemented by two methods.

One method for electrode patterning can be aimed by a particle blasting process. The topography of the electrode working faces depends on the blasting material used. Two blasting materials (glass beads (GB) and glass granulate (GG)) are tested (Fig. 3).

The determination of the process parameters is empirical and assumes the following objectives. The patterning must have a coverage ratio of > 95%. In addition, the resulting surface roughness must be similar. For the particle blasting process, a nozzle with an 8-mm diameter is positioned at a distance of 25 mm from the substrate surface. The patterning of an electrode is carried out with a mass flow of 100 g/min. The pressure in the blasting process is adjusted depending on the respective particle geometry. Analysis of the blasting material by laser diffraction spectrometry yields an average particle diameter of 661 µm (GB) and 346 µm (GG). Related to an ideal spherical shape, the equivalent diameters of the particles are 613 µm (GB) and 170 µm (GG). Taking the particle geometry into account, a process pressure of 6.5 bar (GB) or 5.5 bar (GG) is selected. The process time for the blasting operation is 38 s. The lower process pressure for the GG blasting material is due to the higher abrasive effect of the particles. The resulting topographies of the patterning are analyzed using confocal laser scanning microscopy (CLSM) (Fig. 4).

Both topographies differ in appearance but achieve a comparable surface roughness. A surface roughness R_z of 19.2 µm (GB) and 20.8 µm (GG) is achieved. The maximum roughness depth R_{max} corresponds to 65 µm (GB) or 63.4 µm (GG).

Another method of patterning is implemented by contour turning. The electrode working faces have the global geometry according to ISO 5821 A0-16-20-100. A multi-ring geometry is achieved by overlaying a local geometry (trapezoidal shape). The length of a trapezoidal segment is 0.3 mm. Thus, the overall geometry consists of ten rings, which are globally curved around the radius of 100 mm. The local geometry depth is 0.1 mm (MR100) or 0.2 mm (MR200) (Fig. 5).

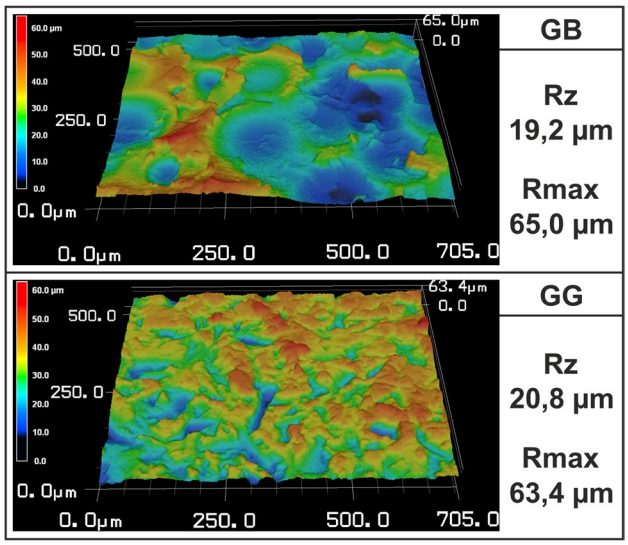

Fig. 4 Topography of patterned electrode working faces GB and GG—initial state (CLSM)

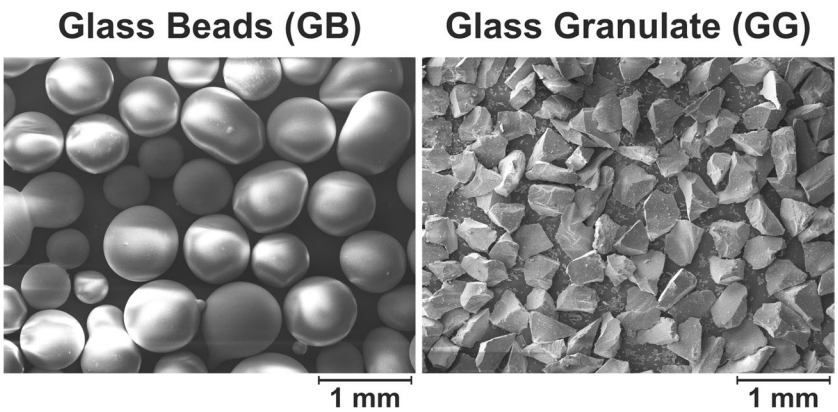

Fig. 3 Blasting materials for patterning electrode working faces—sodium silicate glass

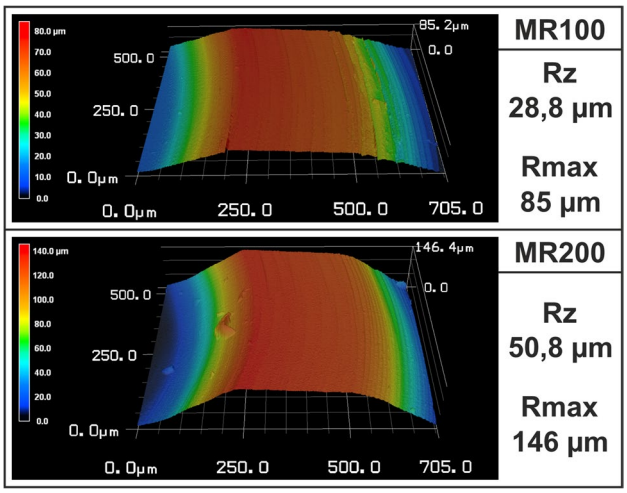

Fig. 5 Topography of patterned electrode working faces MR100 and MR200—initial state (CLSM)

Table 1 Coating materials—electrical and thermal conductivity

	Ni	TiB_2	W
Electrical conductivity in S/m	$14.3 \cdot 10^6$	$3.5 \cdot 10^6$	$18.9 \cdot 10^6$
Thermal conductivity in W/(m·K)	91	64	174

The multi-ring (MR) geometry is implemented in two configurations that differ in their respective trapezoidal depths. The MR geometries produce a surface roughness R_z of 28.8 µm (MR100) and 50.8 µm (MR200). The maximum roughness depth R_{max} is 85 µm (GB) or 146 µm (GG).

4.3 Generating of thin-film diffusion barriers

The generation of thin-film diffusion barriers is intended to prevent direct Al-Cu contact in the welding process. This should inhibit the diffusion processes between the two elements and slow down the degradation of the electrode working faces. In the following, the coatings nickel (Ni), titanium diboride (TiB_2), and tungsten (W) generated by physical vapor deposition (PVD) will be investigated. These thin-film diffusion barriers show high potential to inhibit diffusion processes of the Al-Cu contact pair [15, 16]. The selection of these coating materials is based on their high electrical and thermal conductivities, high adhesion strength, and high thermal shock resistance. Electrical and thermal properties of the coating materials used are shown in Table 1.

The individual coating thickness is measured optically by scanning electron microscopy (SEM). A focused ion beam (FIB) is used to cut out a characteristic part of the material section. This allows the structure of the individual coating to be analyzed without thermal or mechanical load (Fig. 6).

The diffusion barriers show complete bonding to the substrate material. The layer structure is dendritic and reaches layer thicknesses of about 3.0 µm (Ni), 0.6 µm (TiB_2), and 1.6 µm (W).

Investigation of the coated electrodes by GI-XRD (Fig. 7) shows the presence of crystalline phases (fcc Ni, Fm3m, hexagonal TiB_2, P6/mmm, and bcc W, Im-3m) without any impurity phases. The enhanced width of the Bragg peaks corresponding to TiB_2 indicates a nano-crystalline structure with grain sizes of about 10 to 20 nm.

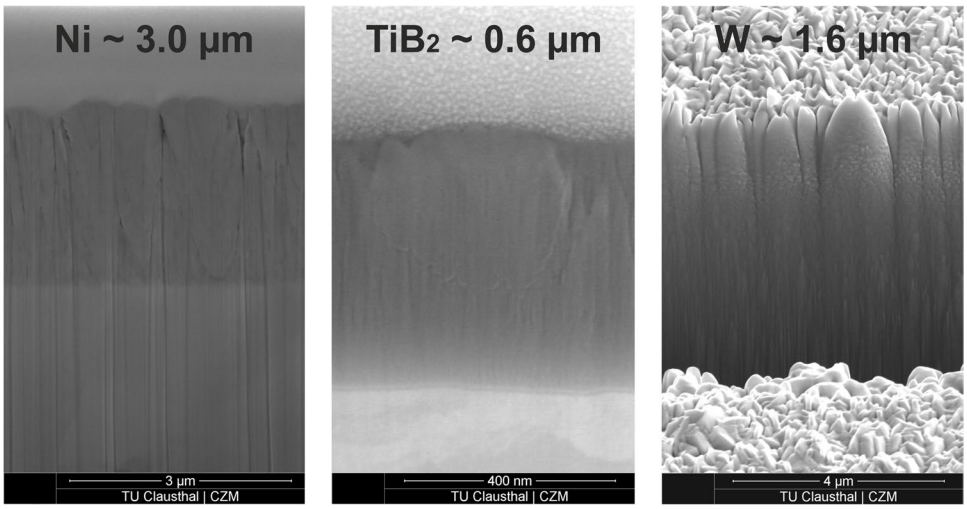

Fig. 6 Thin-film diffusion barriers (PVD)

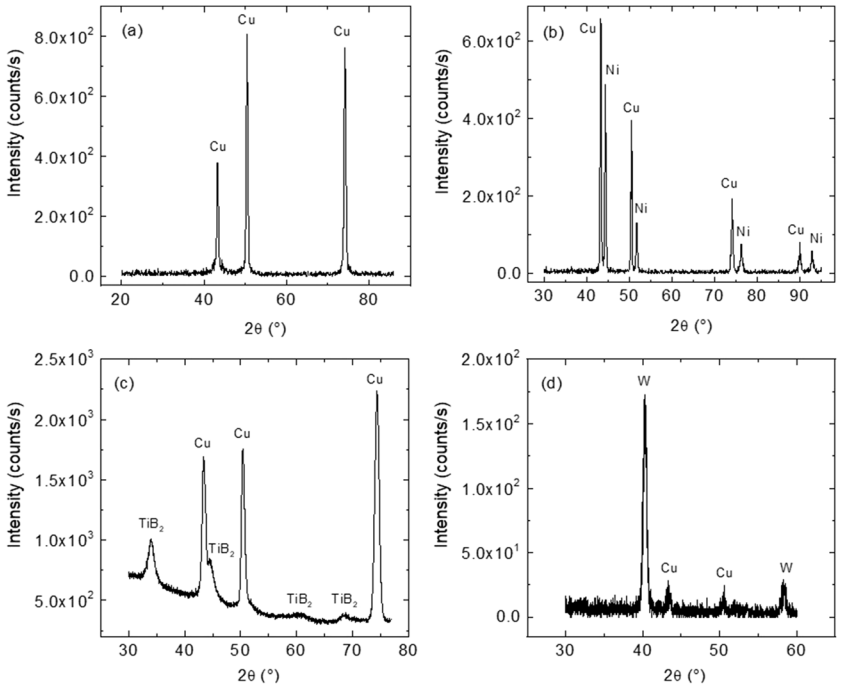

Fig. 7 GI-XRD patterns of the electrode caps **a** without coating and coated with **b** Ni, **c** TiB2, and **d** W. The corresponding phases are indicated. The low intensity of the Cu peaks in (d) is due to the high absorption of the W layer

Table 2 Welding parameters for electrode life studies

Electrode Force	Squeeze Time	Current	Weld Time	Hold Time
3 kN	300 ms	25 kA	50 ms	300 ms

5 Results and discussion

5.1 Welding experiments

In the first step, standard electrode caps R100 (ISO 5821 A0-16-20-100) are used for welding experiments. The experiments are based on two sheet metals (AlMg3 – 3.3535) with 1 mm thickness each and electrode caps (CuCr1Zr–2.1293). For the determination of the electrode life, 50 weld cycles are carried out in each case. The welding parameters used are shown in Table 2.

The selected process variables correspond to the specifications of guideline DVS 2932-3. For processing the alloy AlMg3 with a single sheet thickness of 1 mm, a weld current of 25 kA, 60 ms weld time, and 3 kN electrode force are recommended [17]. This process range is also used by other authors for the corresponding sheet thickness [18]. However, there is no international standard or guideline for the definition of welding parameters. Due to the limited performance capability of the resistance welding machine used, the weld time is reduced to 50 ms. Within the electrode life studies, different degradation effects occur. After the first weld cycle, the electrode working face is chemically melted partially. This is due to the weld nugget reaching the boundary of the electrode/sheet contact. Further weld cycles cause a crack formation in the outer sheet surface (2nd weld cycle), pitting effects on the electrode working face (3rd weld cycle), formation of weld spatters (11th weld cycle), and direct bonding between the electrode and the sheet metal (42th weld cycle).

The minimum weld diameter is defined by $4\bullet\sqrt{t}$ (t: smallest sheet thickness in mm) and the recommended weld diameter by $5\bullet\sqrt{t}$ [19]. Other guidelines recommend a weld diameter of $5.5\bullet\sqrt{t}$ [18]. Within the series of experiments, there is no dropping below the minimum weld diameter limit. The occurrence of weld spatter in the electrode/sheet contact leads to the formation of defects in the joint cross-section and accelerates the degradation of the electrode working faces. Therefore, the formation of weld spatter in the contact area is defined as the abort criterion.

5.2 Process behavior of patterned electrode working faces

Besides the high degradation effects of the standard electrode caps R100, high variations occur in the resulting weld diameters (Fig. 8).

For the first weld cycles, a continuous growth of the weld diameter by constant welding parameters occurs. This can be explained by diffusion effects in the electrode working faces, whereby the decreasing electrical conductivity results in higher heat generation in the electrode/sheet contact. Because the correlation between the electrical energy per weld cycle and the resulting weld diameter is low (r^2 =

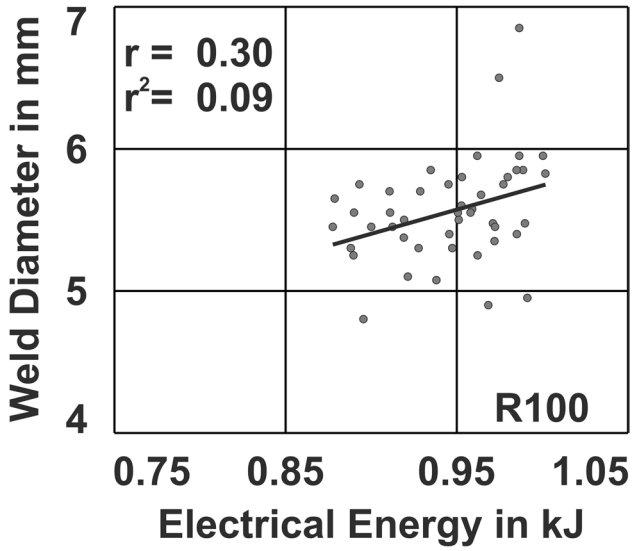

Fig. 8 Regression between the electrical energy per weld cycle and the resulting weld diameter—standard electrode caps R100

0.09), there is an insufficient reproducibility by the usage of standard electrode caps R100. The use of patterned electrode working faces leads to an increase in the coefficient of determination (Fig. 9).

For all patterned electrode working faces, the coefficient of determination can be increased within the welding experiments—GB ($r^2 = 0.66$), GG ($r^2 = 0.34$), MR100 ($r^2 = 0.25$), and MR200 ($r^2 = 0.64$). With constant welding parameters, significantly smaller spot diameters are achieved for GB and GG (particle blasting process). At the same time, the amount of electrical energy per weld cycle is also reduced. In direct comparison, the amount of electrical energy and the resulting weld diameter are higher for MR100 and MR200 (contour turning process).

The lowest correlation is achieved for GG and MR100. This suggests that a change in current flow paths occurs between different welds. With each weld cycle, there is a change in current density that results in a high variation in weld diameters. It is assumed that the fine structure GG plasticizes, due to the mechanical stresses in the welding process, and thus, a change in the electrode/sheet contact area occurs (Fig. 10).

Within the first ten weld cycles, the GB and GG patternings are negatively affected. The surface roughness is reduced by about 21% (GB) or 14% (GG). The highest parts of the topography are wetted with aluminum and deforms. It can be assumed that these structures tend to plasticize due to the high surface-to-volume ratio. With an equal number of weld cycles, this does not occur with the MR100 or MR200 patternings.

All the patternings investigated significantly reduce the electrical contact resistance between the electrodes and the sheet material (Fig. 11). The electrical resistance of the MR100 patterning is increased by a factor of 2 compared to MR200. The reason for this is the reduced profile depth (0.1 mm). This reduces the relative movements occurring between the electrode working face and the sheet surface.

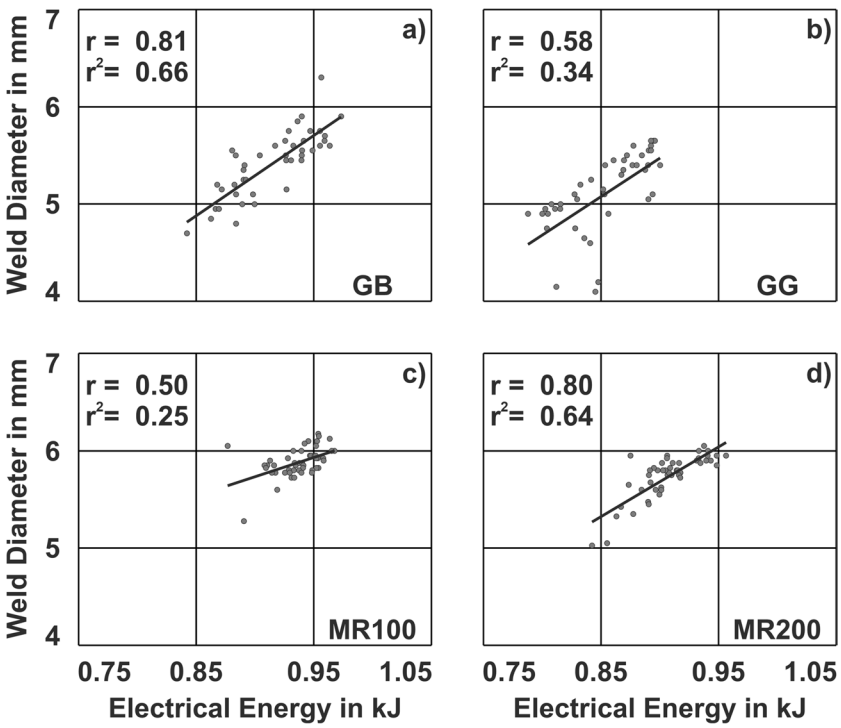

Fig. 9 Regression between the electrical energy per weld cycle and the resulting weld diameter—patterned electrode working faces

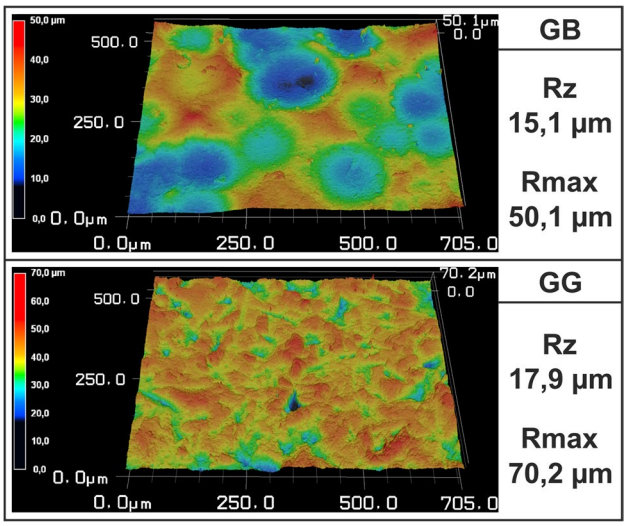

Fig. 10 Topography of patterned electrode working faces GB and GG after ten weld cycles (CLSM)

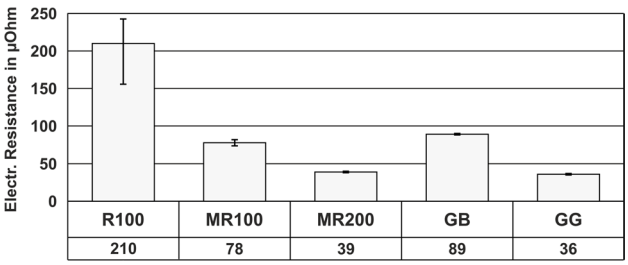

Fig. 11 Static electrical resistance between electrodes—1 × 1 mm AlMg3

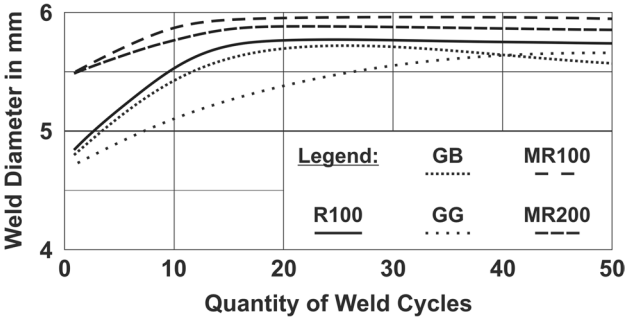

Fig. 12 Electrode life experiment—resulting weld diameter

As a result, higher proportions of aluminum oxide remain in the electrical contact. Further influences of the different patterning can be described on the basis of the achieved weld diameter (Fig. 12).

Using the same process parameters, the resulting weld diameters of the tested electrodes differ significantly. Standard R100 electrodes show a continuous increase in the weld diameter within the first 15 weld cycles. Thereafter, an average weld diameter of approx. 5.7 mm is achieved.

At the 25th weld cycle, the GB patterning reaches the maximum weld diameter of 5.6 mm. Further weld cycles lead to a reduction of the weld diameter. The increase of the achievable weld diameter of the GG pattern is not yet completed after 50 weld cycles. The GB and GG patternings (blasting process), therefore, show an unfavorable process behavior. The MR100 and MR200 patterning also show an increase in the weld diameter in the range of low weld cycles. However, the maximum weld diameter is already reached between 12 and 15 weld cycles. Thereafter, the average weld diameter remains constant at 5.9 mm (MR100) and 5.8 mm (MR200).

The maximum weld diameter is reached after only a few weld cycles and is kept constant on average over further cycles. Therefore, the process behavior of the MR100 and MR200 patterning (contour turning process) can be rated as advantageous compared to the particle blasting process. The process behavior can be described in more detail by the electrical energy per weld cycle (Fig. 13).

The energy quantities shown correspond to the average value of the first ten weld cycles in each case. The energy quantities are shown separately for each interface (anode/sheet, sheet/sheet, cathode/sheet). The electrical energy per weld cycle is 0.928 kJ for the reference R100. The use of patterned electrode working faces reduces the electrical energy per weld cycle. The reduction of the electrical energy depends on the individual patterning: GB (−5.3%), GG (−17.2%), MR100 (−2.1%), and MR200 (−11.5%). The amounts of electrical energy in the electrode/sheet contact are also reduced. Therefore, the patterning contributes to destroying the aluminum oxide layer in the contact area.

The GB and GG patternings have certain disadvantages compared with MR100 and MR200. After only a few weld cycles, there is a deformation/degradation in the topography (Fig. 10). This makes combined use with thin-film diffusion barriers more difficult. High plastic deformation of the patterning could lead to an early delamination of the coating, especially for diffusion barriers with high hardness. Furthermore, smaller weld diameters are achieved overall (Fig. 12). In some cases, these weld diameters fall below the recommended specification of $5 \cdot \sqrt{t}$. Compensation of the smaller weld diameters for the GB and GG patternings by adjusted process parameters was not pursued at this point. In particular, the exclusive influence of the patterning on the fluctuation range of the resulting weld diameters needed to be investigated. Since the MR200 pattern shows the best process behavior and is also suitable for diffusion barriers due to its topography, it will be used as the favored geometry in the following. The influence of the GB and GG patternings on the achievable electrode life is to be investigated in the future on suitable welding machines.

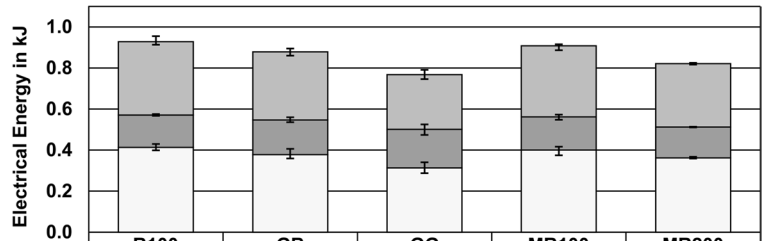

	R100	GB	GG	MR100	MR200
Cathode/Sheet	0.357	0.332	0.267	0.347	0.309
Sheet/Sheet	0.158	0.169	0.188	0.157	0.150
Anode/Sheet	0.413	0.378	0.313	0.405	0.362
Σ	0.928	0.879	0.768	0.909	0.821

Fig. 13 Electrical energy per weld cycle—patterned electrode faces

5.3 Combined use of electrode patterning and thin-film diffusion barriers

The patterning MR200 is coated by PVD with thin-film diffusion barriers, which should contribute to a further improvement of the process behavior. The coatings Ni (3.0 µm), TiB_2 (0.6 µm), and W (1.6 µm) are investigated. The coating thickness selected depends on the respective electrical and thermal conductivities. Because tungsten tends to brittle behavior, the coating thickness was limited to prevent a possible delamination. In order to provide good comparability of the results, the respective weld current is adjusted until a similar electrical energy per weld cycle is obtained (~0.9 kJ) (Fig. 14).

TiB_2 and W increase the amount of electrical energy per weld cycle. For the realization of comparable process conditions, a reduction of the weld current to 22 kA is required for these coatings. The effect of Ni-coated MR200 electrodes on the electrical energy is low. In the welding process, the electrical energy is increased by about 7.3% compared to uncoated MR200 electrodes. The influence of the coatings on the degradation process is shown in Fig. 15.

Standard R100 electrodes already degrade after the first weld cycle. Diffusion processes occur in the contact area, and the electrode working face is partially wetted with aluminum. Therefore, the degradation process occurs rapidly. When using the MR200 patterning, there are significantly reduced diffusion processes in the electrode/sheet interface. Chemical melting of the electrode working face and pitting occurs with a strong delay compared to the reference R100. Therefore, material bonds in the electrode/sheet contact are also reduced during the welding process, which can be attributed to the occurrence of chemical melting.

The additional use of diffusion barriers has different influences on the degradation process depending on the coating material. Coatings with TiB_2 generate a high amount of electrical energy per weld cycle. It is assumed that the resulting high thermal load on the electrode working faces accelerates the degradation process of the TiB_2 coating.

W contributes to a slight reduction in the degradation process. Early wetting of aluminum (1st weld cycle) occurs, leaving the diffusion barrier undamaged. Pitting occurs for the first time after 10 weld cycles. The condition of the electrode working face is only slightly improved compared to uncoated MR200 electrodes. After 25 and 50 weld cycles, the degradation state is the same as for the MR200 electrodes.

Ni coatings lead to a significant reduction of the degradation processes. First weld spatter occurs with the 23rd weld cycle (MR200+Ni). Pitting leads to local damage of the diffusion barrier after the 25th weld cycle. Despite the damaged diffusion barrier, further degradation progress remains

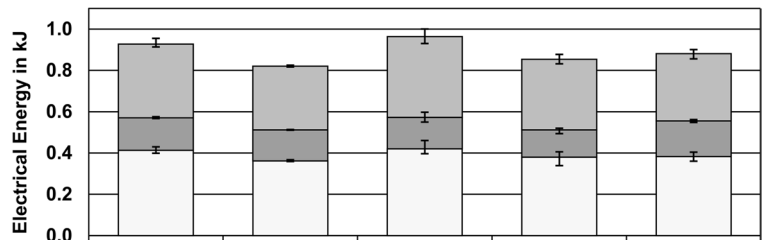

	R100 25 kA	MR200 25 kA	MR200 + 0.6 µm TiB2 22 kA	MR200 + 1.6 µm W 22 kA	MR200 + 3.0 µm Ni 25 kA
Cathode/Sheet	0.357	0.309	0.392	0.341	0.326
Sheet/Sheet	0.158	0.150	0.152	0.132	0.172
Anode/Sheet	0.413	0.362	0.420	0.380	0.383
Σ	0.928	0.821	0.964	0.853	0.881

Fig. 14 Electrical energy per weld cycle—MR200 patterning with different thin-film diffusion barriers

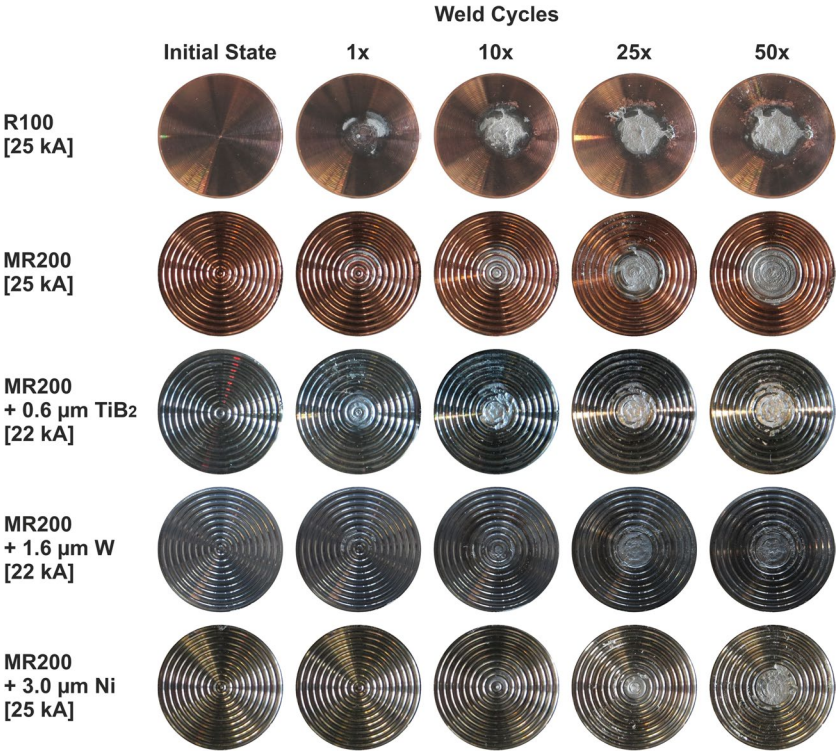

Fig. 15 Macroscopic images of patterned electrode working faces (anode side) at different quantities of weld cycles

slowed down. The electrode life compared to the reference R100 is thus increased by about 100% (abort criteria: weld spatter).

The MR100 and MR200 patternings achieve a higher weld quality even without the combined use of a Ni coating. However, the attainable electrode life is in the range of the reference R100 (8–12 welding cycles). For the diffusion barriers W and TiB_2, further investigations are necessary in the future so that an improvement in weld quality can be achieved compared to MRD200+Ni. The achieved weld qualities of the pattern MR200 as well as the reference R100 are shown in combination with the diffusion barriers in Fig. 16.

The welded joints of the 10th weld cycles are shown in cross-sections. The mean weld diameter $\overline{D}$ and the standard deviation σ result from the adjacent welds (9th, 11th, and 12th weld cycles). The elliptical shape of the spot weld is recorded by two orthogonal measurements within the chisel test. Pores and internal cracks occur in the weld cross-section of the reference R100. The weld nugget also partially reaches the outer sheet surface, which means that the risk of weld spatter formation is increased. The MR200 patterning can reduce the imperfections (pores and cracks) by achieving a comparable weld diameter $\overline{D}$. In addition, the weld nugget height is reduced. Therefore, the thermal load on the electrode working faces and the degradation effects are also reduced.

The TiB_2 and W coatings cause melting of the outer sheet surface despite a reduced weld current (22 kA). As a

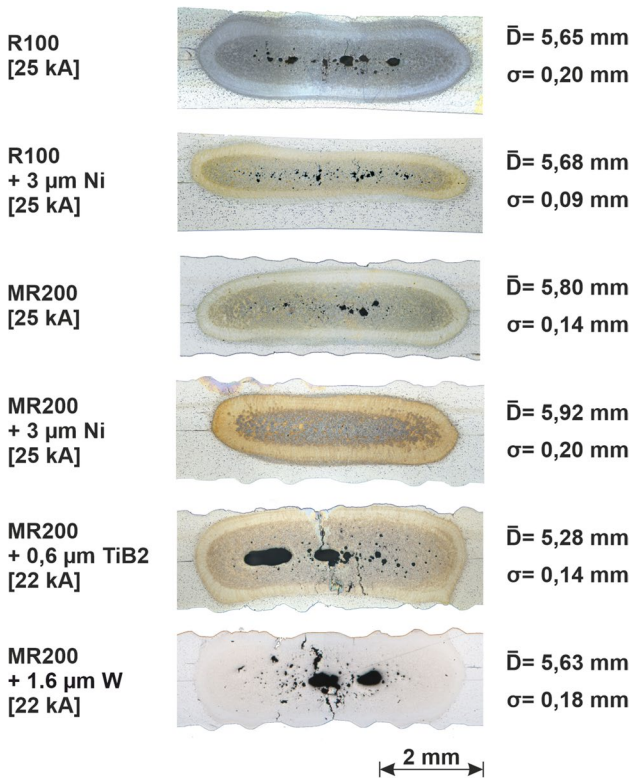

Fig. 16 Microscopic images of weld cross-sections (NaOH etched)—MR200 geometry and thin-film diffusion barriers

result, weld spatter occurs at an early stage in the electrode life study. The consequence is low joint quality (pores and cracks). Furthermore, the direct contact of the electrode working face with molten aluminum phase causes a high thermal load and diffusion rate. The formation of weld spatter in the electrode/sheet interfaces and the resulting wetting of the electrode working faces with aluminum further increase the degradation rate.

MR200 electrodes with Ni coatings achieve the best joint quality. No defects (pores or cracks) are visible in the weld cross-section. The low weld nugget height contributes to a low thermal load on the electrode working faces and a low risk of weld spatters. As a result, high electrode life can be achieved. Due to the elliptical shape of the weld joint, the nugget diameter shown in the cross-section may be smaller than the resulting weld diameter.

6 Conclusion

Resistance spot welding of aluminum alloys with conventional resistance welding machines with limited performance capability (low electrode force and weld current) leads to an insufficient electrode life and weld quality. Standard R100 electrodes show degradation effects after the first weld cycle. Diffusion processes occur in the electrode/sheet contact, resulting in local chemical melting of the electrode material and the formation of intermetallic phases. This leads to the formation of weld spatter in the electrode/sheet contact, which reduces the weld quality and increases the degradation rate.

The use of patterned electrode working faces reduces the electrical contact resistance and the thermal load in the electrode/sheet contacts. However, patterning by a particle blasting process (GB and GG) shows unfavorable process behavior. By the same process parameters, the resulting weld diameter is reduced. In addition, there is a continuous change in weld diameters with increasing weld cycles. Patterning by contour turning process (MR100 and MR200) leads to an increase in the resulting weld diameter compared to the reference R100. Furthermore, the weld diameter remains constant over several weld cycles. It is assumed that the multi-ring geometries achieve homogeneous current conduction with simultaneously high current density. Thus, the contact resistances can be reduced, and at the same time, higher weld diameters can be achieved. Due to the lower variations, the MR200 geometry (0.2 mm profile depth) achieves the best results.

The influence of thin-film diffusion barrier coatings on the welding process depends on the coating materials. TiB_2 (0.6 µm) leads to a high amount of electrical energy per weld cycle. As a result, there is a high thermal load of the electrode working faces resulting in higher degradation rates. W (1.6 µm) leads to only a slight reduction in the degradation rate. The reason for this is the critical height of the weld nugget, melting the outer sheet surfaces. As a result, the electrode working face comes into direct contact with molten aluminum, which greatly increases the degradation rate. At the same time, weld spatter is formed in the electrode/sheet contact. The electrodes are wetted with molten aluminum, which negatively affects the process behavior of subsequent weld cycles. Ni (3.0 µm) significantly increases both the electrode life and the weld quality. When the initial formation of weld spatter is defined as the abort criterion, MR200 electrodes with Ni coating can increase the electrode life by about 100%.

In further investigations, the suitability of conventional resistance welding machines with limited performance capability for processing aluminum alloys is to be further increased. An adaptation of the patterning should contribute to a further limitation of the weld nugget height. Thus, the thermal load on the electrode working faces shall be reduced over a higher number of weld cycles. It is planned to optimize the individual welding parameters by using a design of experiments and, in particular, to improve the applicability of the W and TiB_2 coatings. The generation of thin-film diffusion barriers in the multilayer design promises to further reduce the degradation effects. The use of multilayer coatings should help to selectively adjust specific properties in the area of the electrode working faces and to further increase the achievable electrode life.

Funding Open Access funding enabled and organized by Projekt DEAL. This work was funded by the Deutsche Forschungsgemeinschaft (DFG, German Research Foundation) – WE 2846/29-1 and SCHM 1569/37-1. The financial support is gratefully acknowledged.

Data availability Data sets generated during the current study are available from the corresponding author on reasonable request.

Declarations

Conflict of interest The authors declare no competing interests.

References

1. DVS 2920 (2000) Widerstandspunkt-, Buckel- und Rollennahtschweißen von Stahlblechen bis 3 mm mit metallischen Überzügen. German Welding Society, Guideline
2. Rashid M, Fukumoto S, Medley JB, Villafuerte J, Zhou Y (2007) Influence of lubricants on electrode life in resistance spot welding of aluminum alloys. Weld J 86:62–70
3. Gáspár M, Dobosy Á, Tisza M, Török I, Dong Y, Zheng K (2020) Improving the properties of AA7075 resistance spot-welded joints by chemical oxide removal and post weld head treating. Weld World 64:2119–2128. https://doi.org/10.1007/s40194-020-00988-y
4. DVS 2932 (1986) Widerstandspunkt- und rollennahtschweißen von Aluminium und Aluminiumlegierungen von 0,35 bis 3,5 mm Einzeldicke – Vorbereitung und Durchführung des Schweißens. Guideline. German Welding Society
5. Heilmann S, Zwahr C, Knape A, Zschetzsche J, Lasagni AF, Füssel U (2018) Improvement of the electrical conductivity between electrode and sheet in spot welding process by direct laser interference patterning. Adv Eng Mater 20(6). https://doi.org/10.1002/adem.201700755
6. Deng L, Li YB, Carlson BE, Sigler DR (2018) Effects of electrode surface topography on aluminum resistance spot welding. Weld J 97(4):120–132. https://doi.org/10.29391/2018.97.011
7. Sigler DR, Carlson BE, Janiak P (2013) Improving aluminum resistance spot welding in automotive structures. Weld J 92:64–72
8. Tan R, Shigekura E, Kidachi S (1988) Electrodes for use in spot welding. Patent DE3844001A1. Honda Motor Co Ltd
9. Wagner R (2014) Welding Electrode. Patent DE102014203160A1. Volkswagen AG
10. Luo P, Dong Z, Mei ZQ, Xie ZX (2012) Strengthening mechanism of TiB2-TiC complex phases coated electrode. Adv Mater Res 433-440:251–255. https://doi.org/10.4028/www.scientific.net/AMR.433-440.251
11. Hicken S (1997) Metallkundliche Untersuchungen zu Verschleißvorgängen an Elektroden beim Widerstandspunktschweißen von Aluminium. Dissertation. RWTH Aachen
12. Heilmann S, Köberlin D, Merx M, Müller J, Zschetzsche J, Ihlenfeldt S, Füssel U (2019) Numerical and experimental analysis on the influence of surface layer on resistance spot welding process for aluminum alloys 5182 and 6016. Weld World 63:1205–1220. https://doi.org/10.1007/s40194-019-00743-y
13. Lukas H, Lebrun N (2004) Al-Mg binary phase diagram evaluation. MSI, Materials Science International Services GmbH https://search.msi-eureka.com
14. Gröbner J (2004) Al-Cu binary phase diagram evaluation. MSI, Materials Science International Services GmbH https://search.msi-eureka.com
15. Junge J, Brechelt S, Wiche H, Wesling V, Schmidt H (2023) Erhöhung der Standmenge beim Widerstandspunktschweißen von Aluminiumlegierungen durch Elektrodenmodifikation, Teil 1: Diffusionssperrschichten. Bull Mater Res Eng 12:302–314 Shaker. ISBN 978-3-8440-9105-2
16. Brechelt S, Wiche H, Junge J, Schmidt H, Wesling V (2023) Erhöhung der Standmenge beim Widerstandspunktschweißen von Aluminiumlegierungen durch Elektrodenmodifikation, Teil 2: Schweißtechnische Charakterisierung. Bull Mater Res Eng 12:315–329 Shaker. ISBN 978-3-8440-9105-2
17. DVS 2932-3 (1986) Widerstandspunkt- und Rollennahtschweißen von Aluminium und Aluminiumlegierungen. Guideline. German Welding Society
18. Ambroziak A, Korzeniowski M (2010) Using resistance spot welding for joining aluminium elements in automotive industry. Arch Civ Mech Eng 10:5–13. https://doi.org/10.1016/S1644-9665(12)60126-5
19. DIN EN ISO 18595 (2007) Resistance welding – spot welding of aluminium and aluminium alloys – weldability, welding and testing. Standardization, Beuth